Author Manuscript

Author Manuscript

Author Manuscript

Author Manuscript

HHS Public Access

Author manuscript

Magn Reson Med. Author manuscript; available in PMC 2016 December 01.

Published in final edited form as:

Magn Reson Med. 2015 December ; 74(6): 1621–1631. doi:10.1002/mrm.25559.

MR Fingerprinting Using Fast Imaging with Steady State Precession (FISP) with Spiral Readout

Yun Jiang[1], **Dan Ma**[1], **Nicole Seiberlich**[1], **Vikas Gulani**[1,2], and **Mark A. Griswold**[1,2]

[1] Department of Biomedical Engineering, Case Western Reserve University, Cleveland, Ohio, United States

[2] Department of Radiology, University Hospitals Case Medical Center, Case Western Reserve University, Cleveland, Ohio, United States

Abstract

Purpose—This study explores the possibility of using gradient echo based sequences other than bSSFP in the magnetic resonance fingerprinting (MRF) framework to quantify the relaxation parameters.

Methods—An MRF method based on a fast imaging with steady state precession (FISP) sequence structure is presented. A dictionary containing possible signal evolutions with physiological range of T_1 and T_2 was created using the extended phase graph (EPG) formalism according to the acquisition parameters. The proposed method was evaluated in a phantom and a human brain. T_1, T_2 and proton density were quantified directly from the undersampled data by the pattern recognition algorithm.

Results—T_1 and T_2 values from the phantom demonstrate that the results of MRF FISP are in good agreement with the traditional gold-standard methods. T_1 and T_2 values in brain are within the range of previously reported values.

Conclusion—MRF FISP enables a fast and accurate quantification of the relaxation parameters, while is immune to the banding artifact of bSSFP due to B_0 inhomogeneities, which could improve the ability to use MRF for applications beyond brain imaging.

Keywords

MR Fingerprinting; FISP; quantitative imaging; relaxation time; spiral

Introduction

Quantification of the relaxation parameters (T_1 and T_2) has been a long-term research interest in MRI community. Compared to qualitative weighted images, quantitative measurements of these parameters could more directly reflect the changes at the cellular level, which could help better detect disease and follow treatment outcomes. In addition,

Correspondence: Mark Griswold, Ph.D.SA Case Western Reserve University 11100 Euclid Ave - Bolwell B121 Cleveland, OH 44106, USA mark.griswold@case.edu Phone: +1-216-844-8085.

Author Manuscript Author Manuscript Author Manuscript Author Manuscript

calculated images with different contrasts could be generated on demand from high quality T_1 and T_2 maps (1).

The gold standard for T_1 mapping is to acquire multiple time points along the signal recovery curve after either an inversion or a saturation pulse. For measuring T_2, the gold standard is a Carr-Purcell-Meiboom-Gill (CPMG) spin echo sequence characterizing the T_2 decay curve at different echo times. Both methods require long acquisition times and are not practical in the clinical setting. Multiple techniques to shorten the acquisition time have been proposed over years (2–7). Several methods that are sensitive to both T_1 and T_2 (8–10) have been published to quantify T_1 and T_2 values simultaneously. It is possible to further accelerate the acquisition by employing parallel imaging, non-Cartesian readouts (11), and compressed sensing (12). However, all previous methods employed a set of fixed flip angles to acquire the signal along the exponential curves. The analytic solution of the expected signal related to T_1, T_2 values, and acquisition parameters, such as repetition time and echo time, is expressed to estimate the relaxation parameters by the non-linear curve-fitting algorithms. Because the T_1 recovery and T_2 decay curves are simply exponential curves, the accuracy and precision of the estimation of these two parameters could be easily affected by any signal variations caused by motion, undersampling artifacts, etc.

Magnetic Resonance Fingerprinting (MRF) (13) is a novel concept in quantitative imaging that aims to overcome many of these limitations. In contrast to a conventional MRI method that acquires the steady state signal with a set of fixed flip angles at a constant repetition time, MRF pursues unique signal evolutions that are sensitive to multiple parameters for different tissue types. By varying the acquisition parameters in the sequence, such as flip angles, repetition time, and readout trajectory, MRF sequence targets to achieve the temporal and spatial incoherence, which is shown to be extremely efficient. The ability to acquire the transient state signal in the MRF sequence saves the extra acquisition time needed for techniques to achieve the steady state, and constantly adds new information as the scan progresses. After acquisition, MRF uses a pattern recognition algorithm to match the acquired signal to an entry from a dictionary of possible signal evolutions created by simulation of the sequence and a range of biologically relevant relaxation parameters. Thus, multiple quantitative parameters (such as T_1, T_2, off-resonance and proton density maps) can be simultaneously retrieved from the data. As the pattern recognition is a statistical process, MRF has the potential to be less sensitive to errors induced by subject motion and undersampling artifacts. Because there is no requirement for the signal evolution, MRF can exploit all degrees of freedom in sequence parameters, which gives near infinite choices in sequence design.

While the balanced SSFP (bSSFP) signal used in the original MRF publication is sensitive to both T_1 and T_2, quantification still could be affected by the banding artifacts resulting from inhomogeneous fields. The long-used Fast Imaging with Steady State Precession (FISP) sequence acquires coherent steady state signals with a constant unbalanced gradient moment in each repetition time. The FISP sequence does not lead to the banding artifacts that are seen in bSSFP. Without any other mechanisms to destroy the coherence of the transverse magnetization (such as RF spoiling), the sequence is sensitive to both longitudinal

Author Manuscript Author Manuscript Author Manuscript Author Manuscript

and transverse relaxation times. It is well known in conventional MR that a FISP sequence can generate different contrasts by varying the flip angle and repetition time (14,15).

The purpose of this work is to achieve rapid quantification of multiple relaxation parameters using the MRF framework, but in a manner that is immune to the banding artifact of bSSFP. Here we demonstrate that accurate quantification of T_1 and T_2 can be achieved simultaneously using a sequence with unbalanced gradient moments while maintaining scan efficiency at a relatively high level.

Methods

Pulse Sequence Design

In this study, the FISP-type sequence was used in the MRF framework. The unbalanced gradient within each repetition time in FISP can be on either the readout, phase encoding or slice-selection direction as long as a minimum of 2π dephasing is achieved within one voxel. With the unbalanced gradient moment, the acquired signal is a sum of spins within the voxel and thus the sequence is immune to the banding artifact that commonly appears in bSSFP sequence.

Figure 1a shows one example of the MRF-FISP sequence with the unbalanced gradient along the slice-selection direction. In this study, we used a SINC waveform RF pulse with 2 ms duration. The time bandwidth product of the RF pulse was set to 8 to minimize the imperfect slice profile. The unbalanced gradient moment in the slice-selection direction achieved 8π dephasing across 5 mm slice thickness within each repetition time. Echo time was 2 ms, which was fixed for all frames.

In this study, the flip angles and the repetition times are designed to meet two criteria. One is to generate different signal shapes for different tissue types to quantify the relaxation parameters. The other is to have smoothly varied signals to ‘see through’ artifacts from undersampling, physiological motion, etc. With the unbalanced gradient, the FISP-type sequence has shorter transient state compared to the bSSFP sequence. Thus FISP acquisition with the pseudorandom flip angles and repetition times does not generate smooth signal shape as the bSSFP sequence does. In order to drive the signal to transit smoothly, variable flip angles have been used in preparation of the pseudo steady state in TSE (16), and the steady state of bSSFP (17). In this study, we used the sinusoidal variation of flip angles to drive the magnetization into a persistent transient state so that the signal is smoothly varied based on the choice of flip angles. The flip angles were generated by repeating the following pattern

$$FA(n) = sin(n\pi/N_{rf}) * FA_{max} \quad [1]$$

where n is the number of flip angles ($1 < n < N_{rf}$), and FA_{max} is the maximum flip angle that is randomly selected between 5° to 90° for each repetition of the pattern. In this work, N_{rf} was set to 200. Therefore, the flip angles sinusoidally ramped up to the FA_{max}, and then ramped down every 200 frames. The signal at the transient state is highly sensitive to the relaxation parameters; therefore, the signals have distinct shapes with different combinations

Author Manuscript Author Manuscript Author Manuscript Author Manuscript

of T_1 and T_2 values. Ten frames with zero degree flip angle were inserted between two periods, which gives time for the magnetization to relax. Different FA_{max} was used in each 200-frame period. This leads to different signal shapes every period based on T_1 and T_2 values.

The repetition time was varied using a Perlin noise pattern (13) and ranged from 11.5 to 14.5 ms. The varied repetition times give additional T_1 and T_2 weighting besides the varied flip angles. Any other smooth varied pattern of repetition time could generate designed weighting for the sequence (18).

The flip angles and repetition times were randomly generated as shown in Figure 1b. This set were used in all experiments presented here (see the Supporting Materials for the values of the flip angles and repetition times).

A variable-density spiral trajectory using minimum-time gradient design (19) with zero moment compensation was used to acquire data. In the current study, the spiral trajectory requires 24 interleaves to fully sample the inner region, and 48 interleaves to fully sample the outer 256×256 region of k-space. One spiral interleaf was used in each TR, and the trajectory was rotated by 7.5° every TR, resulting in a highly undersampled k-space for each frame.

Dictionary

Because of the dephasing gradient within each repetition time, the signal acquired by MRF-FISP is an average of all spins in one voxel. Thus, the simulation of the signal behavior cannot be performed using the single isochromat method used in the original bSSFP MRF. One could use Bloch simulation that incorporates a large number of isochromats, however, this can make the calculation of the dictionary very time prohibitive. Thus, in this work we used instead the extended phase graph (EPG) formalism (20,21). EPG provides a powerful tool to predict the timing and the amplitude of echo formation. In the EPG algorithm, any pulse sequence can be represented by the effects of RF pulses, T_1 and T_2 relaxation, and dephasing due to unbalanced gradient moments. The spin system, affected by the pulse sequence, is described as a discrete set of phase states (22), which makes it an efficient way to simulate the signal evolution with unbalanced gradient for this study. From one repetition to the next in MRF-FISP sequence, the spins experience different flip angles, varied relaxation effects due to different repetition times, and same amount gradient dephasing. This was implemented in Matlab 2012a (The MathWorks, Natick, MA). A dictionary containing 18,838 entries of possible signal evolutions was calculated for a wide range of possible T_1 values (20 ~ 3000 ms with an increment of 10 ms, and 3000 ~ 5000 ms with an increment of 200 ms) and T_2 values (10 ~ 300 ms with an increment of 5 ms, and 300 ~ 500 ms with an increment of 50 ms).

Pattern Recognition

The calculated dictionary and the measured time course were normalized so that each entry has the same sum-squared magnitude. Although many methods are possible, in this study, we used a relatively simple pattern recognition method. The inner products between the

Author Manuscript Author Manuscript Author Manuscript Author Manuscript

normalized measured time course of each pixel and all entries of the normalized dictionary were calculated, and the dictionary entry corresponding to the maximum value of the inner product was taken to represent the closest signal evolution to the one acquired. T_1 and T_2 values were then derived from this entry. The proton density was the scaling factor between the measured signal and the matched signal evolution from the dictionary. The calculation time was about 30 seconds per slice with matrix size of 256×256 in Matlab 2012a under a Windows 7 operation system with an Intel Xeon 2.4 GHz CPU.

Phantom and In vivo experiments

All studies were performed on a Siemens Magnetom Skyra 3T (Siemens AG Medical Solutions, Erlangen, Germany) with a 20-channel head receiver array. All acquired spiral data were reconstructed using NUFFT (23) with a separately measured spiral trajectory (24) that would correct the gradient imperfection, such as from eddy current or gradient delays. Images from individual coils were combined using the adaptive coil combination method (25), and coil-combined images were normalized to coil sensitivy map to migitate the image intensity variation due to the coil sensitivity (26).

To evaluate the performance of MRF-FISP, a phantom study was performed to compare the results with traditional spin echo methods. A phantom of 10 cylindrical tubes with varying concentration of gadolinium and agarose was scanned. A saturation recovery spin-echo (13 TRs ranging from 50 ms to 5000 ms with a TE of 8.5 ms) and a multi-echo spin echo (15 echoes with TEs from 15 ms to 225 ms with a TR of 10 seconds) sequence were performed to quantify T_1 and T_2 values, respectively. T_1 and T_2 values were calculated by a pixel-by-pixel three-parameter nonlinear least squares fitting.

The MRF-FISP experiment was performed with the parameters shown in Figure 1 with a field-of-view of 30×30 cm^2 and a slice thickness of 5 mm. An acquisition of 1000 time points was performed with one spiral arm per repetition time, which yields a total acquisition time of about 13 seconds for one slice of 256×256 matrix size. The signal evolution of each pixel from the highly undersampled images was then compared to the dictionary to generate T_1 and T_2 maps.

To assess the off resonance effect in relaxation quantification of the proposed method, MRF-FISP data were acquired with different shim settings by changing the shimming current along either the X or Y direction. The field maps with different shim settings were measured by a 6-echo gradient echo recalled sequence with the first echo time of 2.32 ms and echo gap of 2.45 ms. T_1 and T_2 values of each shim setting were compared to the results of the traditional spin-echo methods.

To demonstrate how the number of frames affects the quantification of T_1 and T_2, the relaxation parameters were retrieved with increasing number of frames (from 10 to 960 frames with an increment of 50 frames) from the 1000 time point scan, retrospectively. The efficiency of MRF-FISP was compared to the original MRF-bSSFP for estimation of T_1 and T_2 values using a bootstrapped Monte Carlo method (27). A normal acquisition and a separate noise measurement with no RF pulses applied were performed on phantom for both methods. For MRF-FISP, the acquisition parameters were the same as mentioned above. For

Author Manuscript Author Manuscript Author Manuscript Author Manuscript

MRF-bSSFP, we used the same spiral trajectory and flip angles as reported in (13). The spiral trajectory of MRF-bSSFP requires one interleaf for inner 10x10 and 48 interleaves for fully sampled 128x128 matrix size at the field-of-view of 30 × 30 cm^2. Repetition time was 7.84 ms to 10.84 ms, which results in 9.36 seconds acquisition time for 1000 frames. For both methods, the resolutions of T_1 and T_2 are 10 ms and 5 ms in the pre-calculated dictionary. Fifty "pseudo multiple replicas" were created by repeatedly adding randomly resampled noise into the raw data. T_1 and T_2 values were estimated from each replica respectively. The means and standard deviations of T_1 and T_2 along the fifty repetitions were calculated from 5×5 pixels in each tube in the phantom (13). The efficiency of T_1 and T_2 estimation is defined as

$$\Gamma = \frac{T_n}{\sigma_{T_n}\sqrt{T_{acq}}} \quad [2]$$

where T_n (n = 1 or 2) is the mean value of T_1 or T_2, σ_{Tn} is the standard deviation of T_1 or T_2. T_{acq} is the acquisition time (3,27).

To examine the performance of the pattern recognition algorithm at different acceleration rates, fully-sampled data were acquired from the phantom. The data were retrospectively undersampled at the acceleration rates of 4, 12 and 48, where R = 48 is the one spiral per repetition MRF-FISP acquisition. The undersampled data with the fully sampled data were respectively matched to the same dictionary to calculate the relaxation parameters. *In vivo* human brain data were acquired in one volunteer after informed consent with one spiral per repetition acquisition. Two MRF-FISP acquisitions, one with the dephasing gradient moment along the slice selective direction as shown in Figure 1, the other with the gradient moment along the readout direction, and balanced slice selecitve gradient, were performed with same repeition times, flip angles, and echo times.

Results

Figure 2a-c show T_1, T_2, and proton density maps of the phantom generated from the proposed method. The comparison of T_1 and T_2 values of MRF-FISP with the standard spin echo method is shown in Figure 3a and Figure 3b. It demonstrates that T_1 and T_2 values from MRF-FISP are in good agreement with the gold standard method. T_1 and T_2 values and their standard deviations for each phantom tube with increasing acquisition time (the number for frames) are plotted in Figure 3c and 3d, respectively. Between T_1 and T_2 estimation, with the proposed acquisition parameters, fewer frames are needed for T_1 quantification, and T_2 estimation takes more time. For example, for the T_1 value of 1521 ms, the estimated T_1 is 1533±23 ms with the acquisition time of only 3 seconds. For the T_2 value of 130 ms, the estimated T_2 is 130.5±5.6 ms with the acquisition of around 8 seconds. Figure 3e and 3f show the efficiency of MRF-FISP and MRF-bSSFP in estimating relaxation parameters at different T_1 and T_2 values. MRF-FISP has slightly lower efficiency compared to the bSSFP based MRF sequence. However, MRF-FISP still achieves high precision in T_1 and T_2 estimation. For example, for a T_1 value of 400 ms, it achieves a precision of ±1.7 ms (or 0.4%), and for T_2 value of 59 ms, it achieves a precision of ± 0.3 ms (or 0.5%) with the current dictionary resolutions of T_1 at 10 ms and T_2 at 5ms.

Author Manuscript Author Manuscript Author Manuscript Author Manuscript

Figure 4a shows the field maps at different shim settings. Figure 4b shows the correlations of T_1 between the results of MRF-FISP at different shim settings and the results from the spin-echo methods, and Figure 4c shows the correlations of T_2 results. By changing the shimming currents in the X or Y direction, each tube of the phantom had a different off-resonance. This demonstrates that T_1 and T_2 are still able to be quantified by the proposed method with varying off-resonance.

Figure 5 shows a set of representative dictionary entries with a) varied T_1 values from 700 ms to 900 ms with 50 ms gap, and T_2 of 85 ms, b) a fixed T_1 value of 795 ms and varied T_2 values from 60 ms to 100 ms with 10 ms gap.

T_1 and T_2 values and their standard deviations estimated from regions of interest in 10 tubes esimated from the fully sampled data, and its retrospectivly undersampled data of R = 4, 12 and 48 are listed in Supporting Table S1. Figure 6 shows one representive image, the signal curve of one voxel with T_1 of 795 ms and T_2 of 85 ms from spin-echo methods, and its matched dictionary entry from a) the fully sampled data, and retrospectively underampled data at rate of b) 4, c) 12, and d) 48. With increasing the undersampling rate, the reconstructed image becomes dominated by undersampling artifacts, however, the pattern recognition algorithm is still able to find the corresponding dictionary entry with the maximum inner-product. The values of the inner-product of the same example pixel are 0.99589, 0.968207, 0.775906 and 0.412848 at the acceleration rate of 1 (fully sampled), 4, 12, and 48, respectively. The estimated values in same ROI at different acceleration rates from MRF-FISP are 794 ± 13 ms, 801 ± 14 ms, 800 ± 15 ms, and 801 ± 14 for T_1, 84 ± 5 ms, 85 ± 4 ms, 85 ± 3 ms, and 85 ± 3 ms for T_2. With increasing acceleration rate, the value of the inner-product decreases due to more undersampling artifacts. The estimated T_1 and T_2 values are still very close regardless of the undersampling artifacts. Here, with undersampling artifacts, the estimated T_1 values are about 5 ms overestimated which is within one dictionary entry.

Figure 7a shows one of the undersampled images from the MRF-FISP acquisition. The signal intensities over time for one pixel (denoted by the white dot) are plotted in Figure 7a and its matched dictionary entry are plotted in Figure 7b. While both signal intensities periodically increase and decrease every 200 frames due to the sinusoidal variation of flip angles, the undersampling artifacts in the images cause noise-like fluctuations at a higher frequency. However, as shown previously, even the simple template-matching algorithm used here is able to retrieve the corresponding dictionary entry by effectively “seeing through” the undersampling artifacts, as these artifacts do not appear in the dictionary. The estimated T_1 and T_2 values are 760 ms and 65 ms respectively.

T_1, T_2 and proton density maps generated from an asymptomatic volunteer are shown in Figure 8a, 8b and 8c. The acquisition was with an unbalanced gradient moment along the slice selection gradient. Supporting Figure S1 shows the results from the same volunteer with the sequence having an unbalanced gradient along the readout direction. The mean values of T_1 and T_2 of the region-of-interest in white matter and gray matter are within the range of previous literature results (28) as listed in Table 1. The noticeable difference between Figure 8 and Supporting Figure S1 are the estimated values from CSF, which is

Author Manuscript Author Manuscript Author Manuscript Author Manuscript

affected by the pulsation in CSF due to the change of unbalanced gradient direction. T_1-weighted images calculated from the maps in Figure 8 with TR = 250 ms and TE = 2.5 ms are shown in Figure 9a; T_2-weighted images in Figure 9b were calculated using TR = 10000 ms and TE = 90 ms; FLAIR (fluid-attenuated inversion recovery) images calculated with TI = 3600 ms, TE = 90 ms are shown in Figure 9c.

Discussion

Here we describe a FISP-based MRF method that can be used to quantify relaxation parameters. The results from phantom and *in vivo* human brain data suggest that accurate T_1 and T_2 values can be quantified by the proposed method.

Because of its unbalanced gradient within each repetition time, the simulation of the FISP sequence cannot be treated as a single isochromat in Bloch simulation for calculating the dictionary. While simulation of multiple spins is possible, it requires the simulation of hundreds or thousands of spins to achieve high accuracy, which could be time consuming. These results show that the extended phase graph formalism provides an alternative way to calculate the dictionary of MRF acquisition for sequences with the unbalanced gradient. Without the need to consider off-resonance, the dictionary size of FISP is also smaller compared to that of bSSFP at the same resolution of T_1 and T_2 values. This leads to an accelerated calculation time for the pattern-matching algorithm, or a potential increase in the dictionary resolutions of T_1 and T_2 values. While previous study (29) has illustrated that the variable repetition time causes a change in the signal amplitude of the FISP sequence with different off-resonance, our results show that T_1 and T_2 values can be quantified across a range of inhomogeneous B_0 using the MRF approach built upon pattern recognition. Off-resonance could have more effects on the quantitative results if the sequence employs a set of repetition times with stronger fluctuations, however, any effects such as off-resonance or slice-profile imperfections could be modeled and built into the dictionary used for pattern recognition to improve the final determination of the parameters.

The ability to simulate the gradient dephasing along with the RF pulse and the relaxation parameters gives us flexibility to include different type of sequences into MRF framework. This allows the sequence to employ longer repetition times, which could give more flexibility in sequence design, such as longer readout for higher spatial resolution or more variation in repetition times. It could also extend the MRF application to other organs or higher fields where it is potentially challenging for the bSSFP based sequence due to the banding artifact (30). It also has the potential to extend the method beyond MR relaxometry to quantify other physiological parameters, such as perfusion (31) and diffusion (32).

While the unbalanced gradient moment alleviate the banding artifact from bSSFP, FISP based MRF sequences could be affected by the increasing sensitivity to the motion along the unbalanced gradient direction (33). In brain applications, the most noticeable effect is in the cerebrospinal fluid that flows in and out the imaging slice with its long T_2 value. This results in the potential underestimation of the relaxation parameters in CSF in our proposed method.

Author Manuscript Author Manuscript Author Manuscript Author Manuscript

Here we have only shown one of many examples in choices of flip angles and repetition times that are possible with a sequence such as MRF-FISP. We used the sinusoidal variation of flip angles and the pseudorandom repetition time to drive the magnetization into a persistent transient state that is sensitive to the relaxation parameters. The signal is driven to change smoothly so that the undersampling artifacts, physiological motion artifacts, and other artifacts from the systematic imperfection that varies in higher frequency can be 'seen through' in the pattern recognition algorithm. In the current study, the choice of the acquisition parameters was not fully optimized to generate the most efficient sequence. However, the proposed MRF-FISP method inherits the efficiency of the bSSFP-based MRF method and is able to achieve precisions of T_1 and T_2 values of less than 1% within 13 seconds of scan time. While we observed lower efficiency in MRF-FISP compared to MRF-bSSFP, the efficiency of both acquisitions are higher than the values reported in (13). This increase in efficiency can be attributed to the superior MRI hardware used in this study, including a higher main field magnet (3 T in current study, and 1.5 T in previous study (13)) and an improved multichannel array. We believe that a similar acquisition scheme can be used even in noncoherent steady state pulse sequence, such as FLASH, to quantify T_1, T^*_2, or other parameters in the transient state. Optimizing the sequence parameters of MRF sequence will be an on-going effort because the degrees of freedom to design the sequence are nearly unlimited. The consideration of selecting a particular set of parameters for the MRF sequence needs to consider not only the sensitivity to the interesting parameters, but also image quality of parameter maps when the data are undersampled.

The "pseudo multiple replica method" is a robust measurement of noise when a direct measurement experiment is not possible. This approach represents a repeated measurements experiment, as long as the noise is Gaussian distributed. Non-Gaussian noises among the repetitions, such as noise from the instrument drift, physiological motion, and flow artifacts are not represented in this method.

Like all quantitative methods, the estimation of the parameters depends on how accurate the signal model reflects the actual acquired data. Several factors, such as imperfect slice profile, B_1^+ inhomogeneity, and MT effect could affect the estimation of T_1 and T_2 (11,34). In this study, the dictionary was calculated with the ideal slice profile. The actual flip angle could be smaller than the nominal flip angle due to the imperfection of slice profile. In order to minimize the imperfect slice profile, a SINC RF waveform with the time bandwidth produce (TBP) of 8 was used. While the data are acquired using a RF pulse with a worse slice profile, slice profile correction (11) can be employed to mitigate the effect. A previous study (35) also showed the slice profile calculation can be included into EPG formalism to address this issue. An inhomogeneous transmit B_1 field would also affect the actual flip angle across FOV. While it is not severe in the phantom or brain application presented here, it could affect the results in the applications where larger FOV or more complicated coil setup is necessary. Either including B_1 into the dictionary, which is able to estimate B_1 simultaneously with the relaxation parameters (36) or adding an extra B_1 measurement, which matches the acquired signal to the corresponding dictionary with same B_1(30), would improve the quantification accuracy. The early study (30) has shown that B_1 effect in MRF sequence affects T_2 quantification more than T_1 quantification. Magnetization transfer (MT) effect is also known to affect T_1 quantification, especially in variable multiple flip angle

Author Manuscript Author Manuscript Author Manuscript Author Manuscript

methods (37,38). The transient state that MRF acquires is also sensitive to MT (39). The effect of MT is more apparent when using high power RF pulses with a short repetition time. Previous study (40) showed that reducing RF power by prolonging the RF pulse can be effective in reducing MT-related signal loss. MRF-FISP sequence is more flexible in terms of using longer repetition times and RF pulse duration because of the immunity to banding artifacts. In this study, we used RF pulses with 2 ms duration, and 11.5~14.5 ms repetition times, which has the potential to minimize MT effect in the sequence.

Though quantification of other physiological parameters, such as diffusion coefficients or perfusion, is out of scope of the current work, we believe the introduction of unbalanced gradient moment into MRF sequence opens new opportunities to quantify extra parameters besides T_1, T_2, and proton density.

Supplementary Material

Refer to Web version on PubMed Central for supplementary material.

Acknowledgements

The authors would like to acknowledge funding from Siemens Medical Solutions, NIH grants 1R01EB017219, R00EB011527 and 1R01DK098503 and Dr. Brian Hargreaves for his code and assistance with the EPG formalism.

References

1. Cheng H-LM, Stikov N, Ghugre NR, Wright GA. Practical medical applications of quantitative MR relaxometry. J. Magn. Reson. Imaging. 2012; 36:805–24. [PubMed: 22987758]
2. Look DC. Time Saving in Measurement of NMR and EPR Relaxation Times. Rev. Sci. Instrum. 1970; 41:250.
3. Deoni SCL, Rutt BK, Peters TM. Rapid combined T1 and T2 mapping using gradient recalled acquisition in the steady state. Magn. Reson. Med. 2003; 49:515–26. [PubMed: 12594755]
4. Messroghli DR, Radjenovic A, Kozerke S, Higgins DM, Sivananthan MU, Ridgway JP. Modified Look-Locker inversion recovery (MOLLI) for high-resolution T1 mapping of the heart. Magn. Reson. Med. 2004; 52:141–6. [PubMed: 15236377]
5. Zhu DC, Penn RD. Full-brain T1 mapping through inversion recovery fast spin echo imaging with time-efficient slice ordering. Magn. Reson. Med. 2005; 54:725–31. [PubMed: 16086307]
6. Cheng H-LM, Wright GA. Rapid high-resolution T(1) mapping by variable flip angles: accurate and precise measurements in the presence of radiofrequency field inhomogeneity. Magn. Reson. Med. 2006; 55:566–74. [PubMed: 16450365]
7. Heule R, Ganter C, Bieri O. Rapid estimation of cartilage T2 with reduced T1 sensitivity using double echo steady state imaging. Magn. Reson. Med. 2013 DOI: 101002/mrm.24748.
8. Warntjes JBM, Dahlqvist O, Lundberg P. Novel method for rapid, simultaneous T1, T*2, and proton density quantification. Magn. Reson. Med. 2007; 57:528–37. [PubMed: 17326183]
9. Warntjes JBM, Leinhard OD, West J, Lundberg P. Rapid magnetic resonance quantification on the brain: Optimization for clinical usage. Magn. Reson. Med. 2008; 60:320–9. [PubMed: 18666127]
10. Schmitt P, Griswold MA, Jakob PM, Kotas M, Gulani V, Flentje M, Haase A. Inversion recovery TrueFISP: quantification of T(1), T(2), and spin density. Magn. Reson. Med. 2004; 51:661–7. [PubMed: 15065237]
11. Ehses P, Seiberlich N, Ma D, Breuer FA, Jakob PM, Griswold MA, Gulani V. IR TrueFISP with a golden-ratio-based radial readout: fast quantification of T1, T2, and proton density. Magn. Reson. Med. 2013; 69:71–81. [PubMed: 22378141]

Author Manuscript Author Manuscript Author Manuscript Author Manuscript

12. Doneva M, Börnert P, Eggers H, Stehning C, Sénégas J, Mertins A. Compressed sensing reconstruction for magnetic resonance parameter mapping. Magn. Reson. Med. 2010; 64:1114–20. [PubMed: 20564599]
13. Ma D, Gulani V, Seiberlich N, Liu K, Sunshine JL, Duerk JL, Griswold MA. Magnetic resonance fingerprinting. Nature. 2013; 495:187–92. [PubMed: 23486058]
14. Sekihara K. Steady-state magnetizations in rapid NMR imaging using small flip angles and short repetition intervals. IEEE Trans. Med. Imaging. 1987; 6:157–64. [PubMed: 18230442]
15. Gyngell ML. The application of steady-state free precession in rapid 2DFT NMR imaging: FAST and CE-FAST sequences. Magn. Reson. Imaging. 1988; 6:415–419. [PubMed: 3185135]
16. Hennig J, Weigel M, Scheffler K. Multiecho sequences with variable refocusing flip angles: Optimization of signal behavior using smooth transitions between pseudo steady states (TRAPS). Magn. Reson. Med. 2003; 49:527–535. [PubMed: 12594756]
17. Deshpande VS, Chung Y-C, Zhang Q, Shea SM, Li D. Reduction of transient signal oscillations in true-FISP using a linear flip angle series magnetization preparation. Magn. Reson. Med. 2003; 49:151–7. [PubMed: 12509831]
18. Wong, ML.; Wu, EZ.; Wong, EC. Proceeding 22th Annu. Meet. ISMRM; Milan, Italy: 2014. Optimization of Flip angle and TR schedules for MR Fingerprinting.; p. 1469
19. Lee JH, Hargreaves BA, Hu BS, Nishimura DG. Fast 3D imaging using variable-density spiral trajectories with applications to limb perfusion. Magn. Reson. Med. 2003; 50:1276–85. [PubMed: 14648576]
20. Hennig J. Multiecho imaging sequences with low refocusing flip angles. J. Magn. Reson. 1988; 78:397–407.
21. Hennig J. Echoes—how to generate, recognize, use or avoid them in MR-imaging sequences. Part I: Fundamental and not so fundamental properties of spin echoes. Concepts Magn. Reson. 1991; 3:125–143.
22. Weigel M. Extended phase graphs: Dephasing, RF pulses, and echoes - pure and simple. J. Magn. Reson. Imaging. 2014
23. Fessler JA, Sutton BP. Nonuniform fast fourier transforms using min-max interpolation. IEEE Trans. Signal Process. 2003; 51:560–574.
24. Duyn JH, Yang Y, Frank JA, van der Veen JW. Simple correction method for k-space trajectory deviations in MRI. J. Magn. Reson. 1998; 132:150–3. [PubMed: 9615415]
25. Walsh DO, Gmitro AF, Marcellin MW. Adaptive reconstruction of phased array MR imagery. Magn. Reson. Med. 2000; 43:682–90. [PubMed: 10800033]
26. Griswold MA, Walsh D, Heidemann RM, Haase A, Jakob P. The Use of an Adaptive Reconstruction for Array Coil Sensitivity Mapping and Intensity Normalization. Proc. Tenth Sci. Meet. Int. Soc. Magn. Reson. Med. 2002:2410.
27. Robson PM, Grant AK, Madhuranthakam AJ, Lattanzi R, Sodickson DK, McKenzie CA. Comprehensive quantification of signal-to-noise ratio and g-factor for image-based and k-space-based parallel imaging reconstructions. Magn. Reson. Med. 2008; 60:895–907. [PubMed: 18816810]
28. Wansapura JP, Holland SK, Dunn RS, Ball WS. NMR relaxation times in the human brain at 3.0 tesla. J. Magn. Reson. Imaging. 1999; 9:531–8. [PubMed: 10232510]
29. Scheffler K. A pictorial description of steady-states in rapid magnetic resonance imaging. Concepts Magn. Reson. 1999; 11:291–304.
30. Chen, Y.; Jiang, Y.; Ma, D.; Wright; Katherine, L.; Seiberlich, N.; Griswold, MA.; Gulani, V. Proceeding 22th Annu. Meet. ISMRM; Milan, Italy: 2014. Magnetic Resonance Fingerprinting (MRF) for Rapid Quantitative Abdominal Imaging.; p. 561
31. Wright, KL.; Ma, D.; Jiang, Y.; Gulani, V.; Griswold, MA.; Hernandez-Garcia, L. n Proceeding 22th Annu. Meet. ISMRM; Milan, Italy: 2014. Theoretical Framework for MR Fingerprinting with ASL: Simultaneous Quantification of CBF, Transit Time, and T1.; p. 417
32. Jiang, Y.; Ma, D.; Wright, KL.; Seiberlich, N.; Gulani, V.; Griswold, MA. Proceeding 22th Annu. Meet. ISMRM; Milan, Italy: 2014. Simultaneous T1, T2, Diffusion and Proton Density Quantification with MR Fingerprinting.; p. 28

Author Manuscript Author Manuscript Author Manuscript Author Manuscript

33. Santini, F.; Bieri, O.; Scheffler, K. Proc. 16th Annu. Meet. ISMRM; Toronto, ON, Canada: 2008. Flow compensation in non-balanced SSFP.; p. 3124
34. Heule R, Bär P, Mirkes C, Scheffler K, Trattnig S, Bieri O. Triple-echo steady-state T2 relaxometry of the human brain at high to ultra-high fields. NMR Biomed. 2014; 27:1037–45. [PubMed: 24986791]
35. Lebel RM, Wilman AH. Transverse relaxometry with stimulated echo compensation. Magn. Reson. Med. 2010; 64:1005–14. [PubMed: 20564587]
36. Cloos, MA.; Wiggins, C.; Wiggins, G.; Sodickson, DK. Proceeding 22th Annu. Meet. ISMRM; Milan, Italy: 2014. Plug and Play Parallel Transmission at 7 and 9.4 Tesla based on Principles from MR Fingerprinting.; p. 542
37. Ou X, Gochberg DF. MT effects and T1 quantification in single-slice spoiled gradient echo imaging. Magn. Reson. Med. 2008; 59:835–45. [PubMed: 18302249]
38. Mossahebi P, Yarnykh VL, Samsonov A. Analysis and correction of biases in cross-relaxation MRI due to biexponential longitudinal relaxation. Magn. Reson. Med. 2013 DOI: 10.1002/mrm.24677.
39. Gloor M, Scheffler K, Bieri O. Nonbalanced SSFP-based quantitative magnetization transfer imaging. Magn. Reson. Med. 2010; 64:149–56. [PubMed: 20572130]
40. Bieri O, Scheffler K. Optimized balanced steady-state free precession magnetization transfer imaging. Magn. Reson. Med. 2007; 58:511–8. [PubMed: 17763346]

Author Manuscript Author Manuscript Author Manuscript Author Manuscript

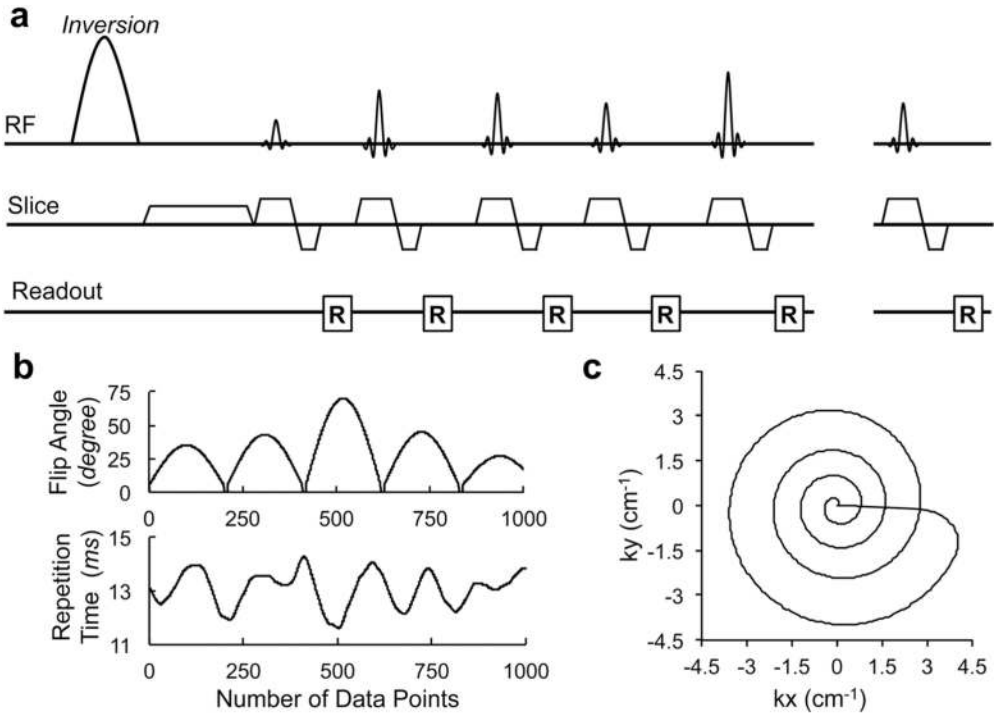

Figure 1.

a: A pulse sequence diagram of the MRF-FISP sequence. An adiabatic inversion pulse is followed by a series of FISP acquisitions. **b:** A sinusoidal variation of flip angles, and repetition times in a Perlin noise pattern, are used in the MRF-FISP sequence. **c:** One interleaf of a variable density spiral trajectory is used in each repetition. The spiral trajectory is zero moment compensated. It needs 24 interleaves to fully sample the center of the k space, and 48 interleaves for 256*256. The trajectory rotates 7.5 degrees every repetition.

Author Manuscript Author Manuscript Author Manuscript Author Manuscript

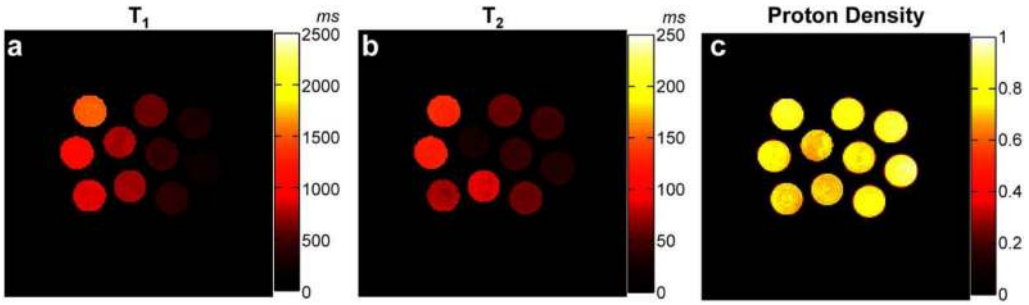

Figure 2.

T_1 (**a**), T_2 (**b**) and proton density (**c**) maps of the phantom with varied concentration of gadolinium and agarose generated using MRF-FISP.

Author Manuscript Author Manuscript Author Manuscript Author Manuscript

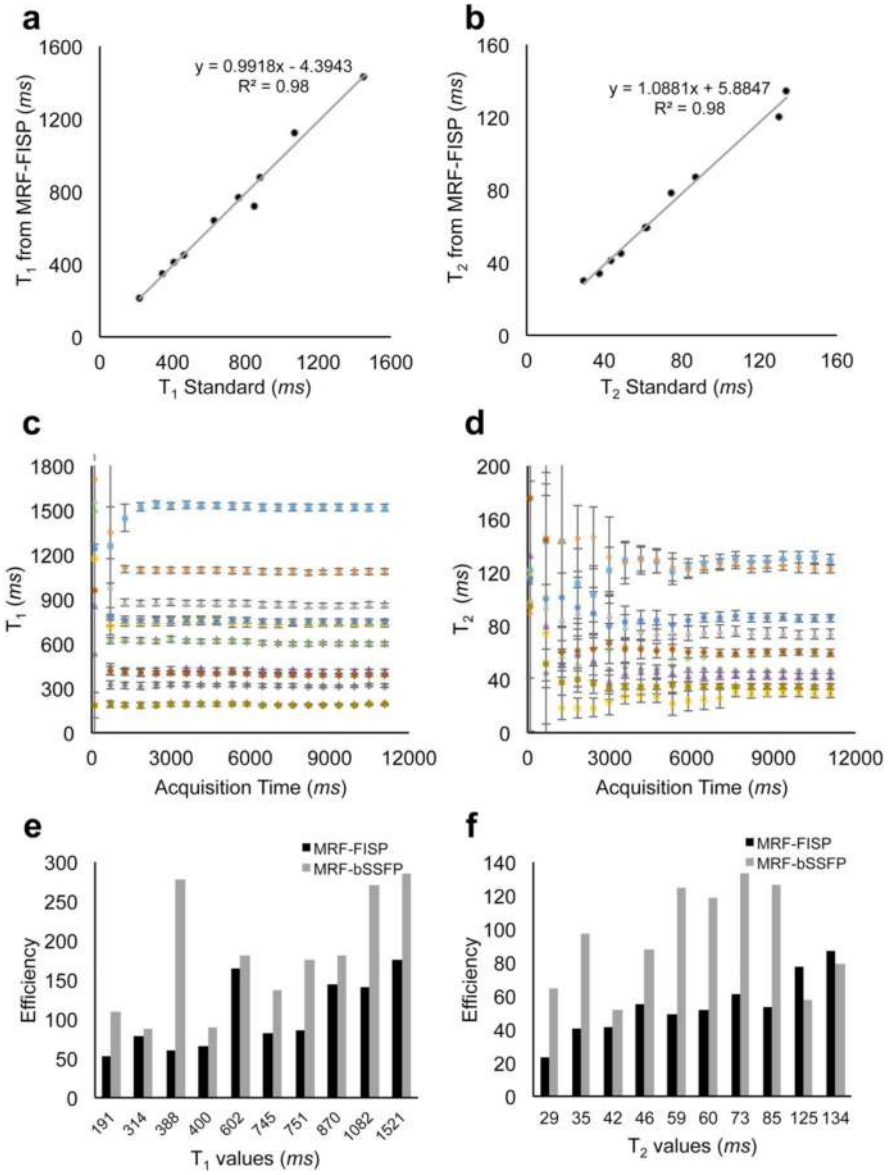

Figure 3.

a-b: The comparison of T_1 (**a**) and T_2 (**b**) values of MRF-FISP with the standard spin echo methods. **c-d:** T_1 and T_2 values and their standard deviations measured by MRF-FISP for each tube with increasing acquisition time (the number for frames). **e-f:** The efficiency of MRF-FISP compared to the efficiency of MRF-bSSFP at different T_1 and T_2 values.

Author Manuscript Author Manuscript Author Manuscript Author Manuscript

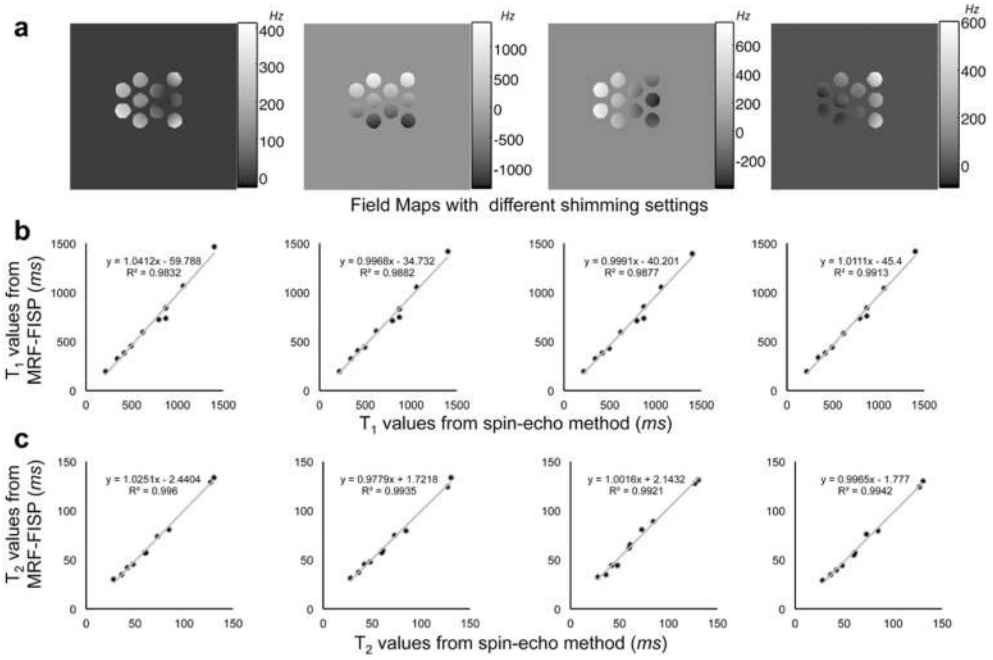

Figure 4.

a: The field maps at different shim settings. The correlations of T_1 (**b**) and T_2 (**c**) between the results of MRF-FISP at different shim settings and the results from the spin-echo methods.

Author Manuscript Author Manuscript Author Manuscript Author Manuscript

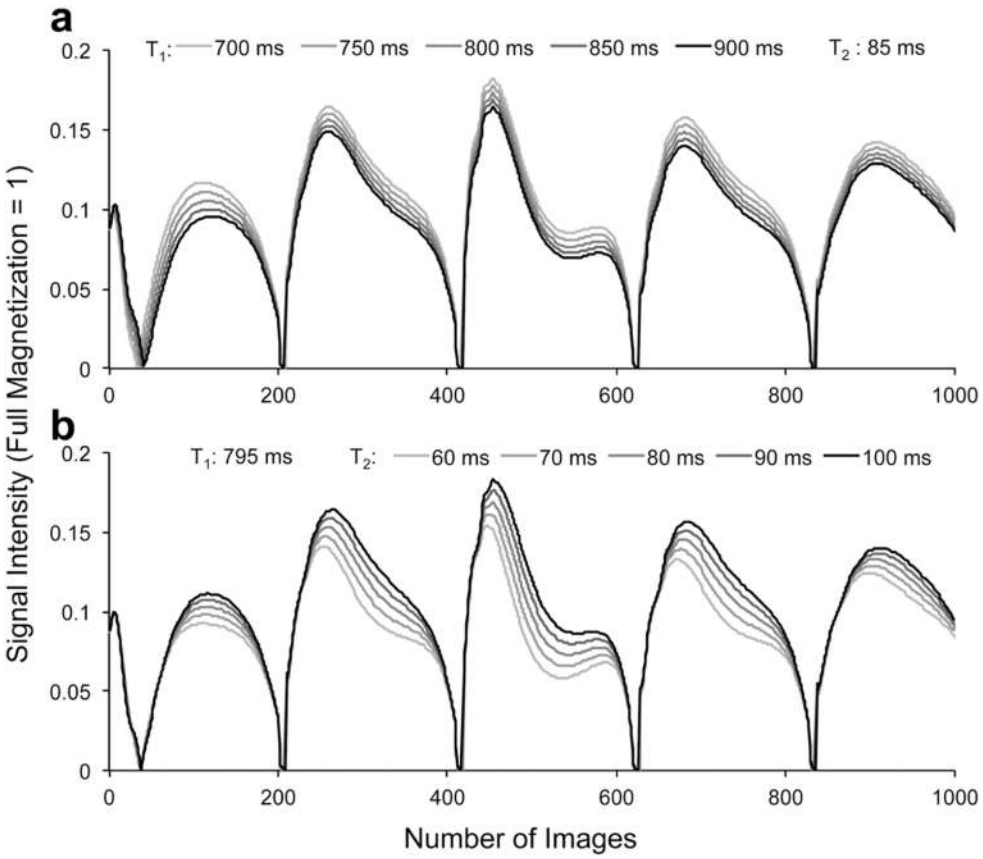

Figure 5.

A set of representative dictionary entries with **a**) T_1 values from 700 ms to 900 ms with 50 ms gap, and T_2 of 85 ms, **b**) a fixed T_1 value of 795 ms and T_2 values from 60 ms to 100 ms with 10 ms gap.

Author Manuscript Author Manuscript Author Manuscript Author Manuscript

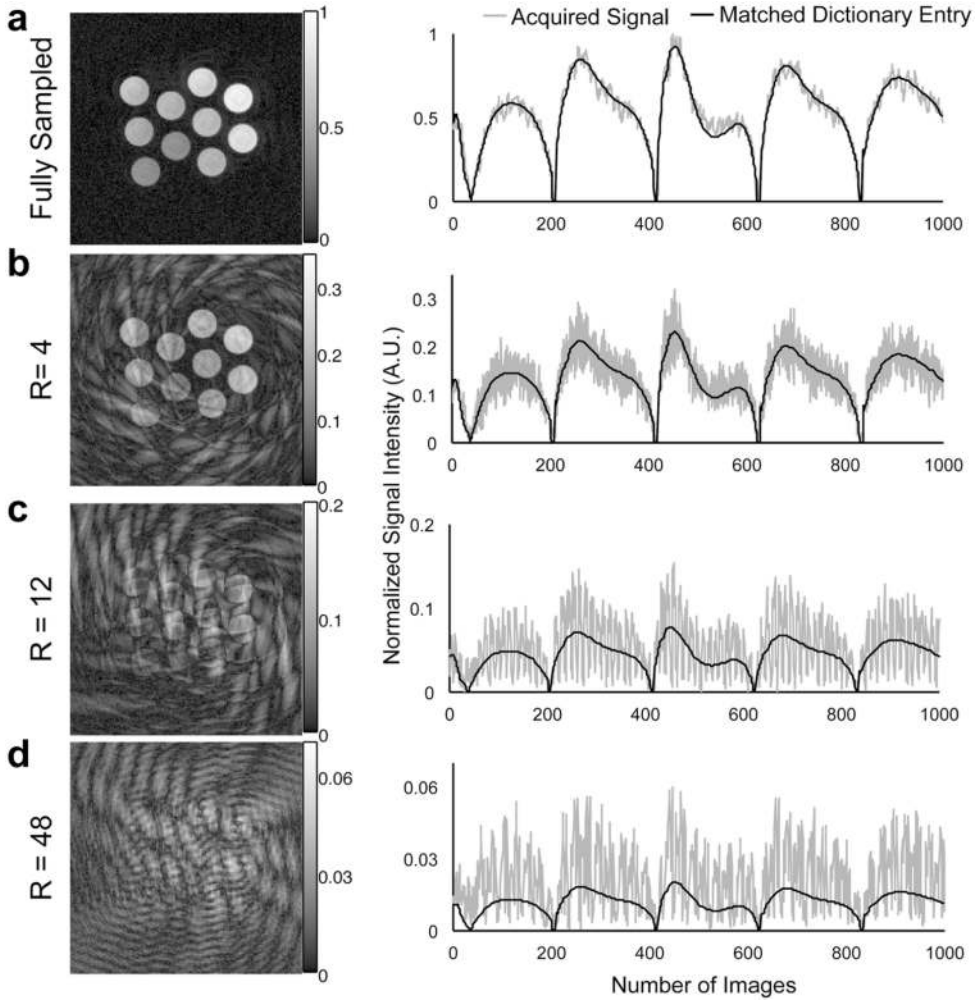

Figure 6.

The representative images, the signal curves of one voxel with T_1 of 795 ms and T_2 of 85 ms, their matched dictionary entries from a fully sampled data (**a**), and retrospectively undersampled data at rate (R) of 4 (**b**), 12 (**c**), and 48 (**d**). For comparison of the signal-to-noise ratio among the data with different R, the plotted signals were normalized to the maximum of the fully sampled data.

Author Manuscript Author Manuscript Author Manuscript Author Manuscript

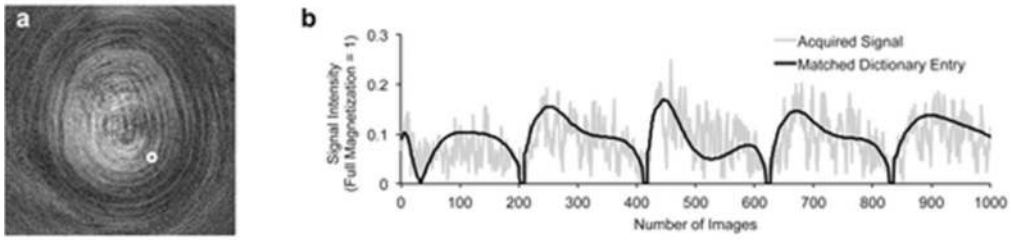

Figure 7.

a: An example of the undersampled images from MRF-FISP. **b**: A representative time course of one pixel as indicated by the white circle in (**a**) and its matched dictionary entry. The estimated T_1 and T_2 values of this pixel are 750 ms and 65 ms, respectively. The longitudinal axis represents the fraction of the full magnetization that is equal to one.

Author Manuscript Author Manuscript Author Manuscript Author Manuscript

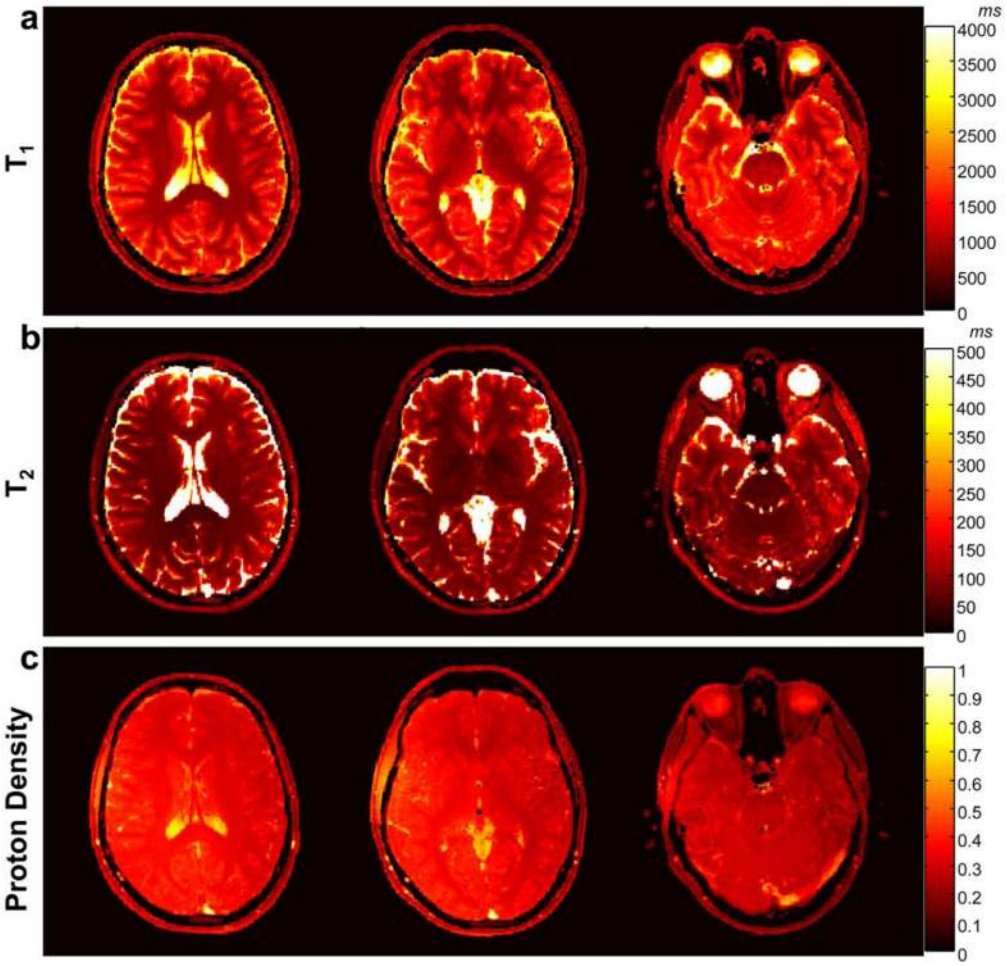

Figure 8.

T_1 (**a**), T_2 (**b**) and proton density maps (**c**) generated from an asymptomatic volunteer with the MRF-FISP acquisition. The unbalanced gradient moment along the slice selection gradient achieves 8pi dephasing per voxel.

Author Manuscript Author Manuscript Author Manuscript Author Manuscript

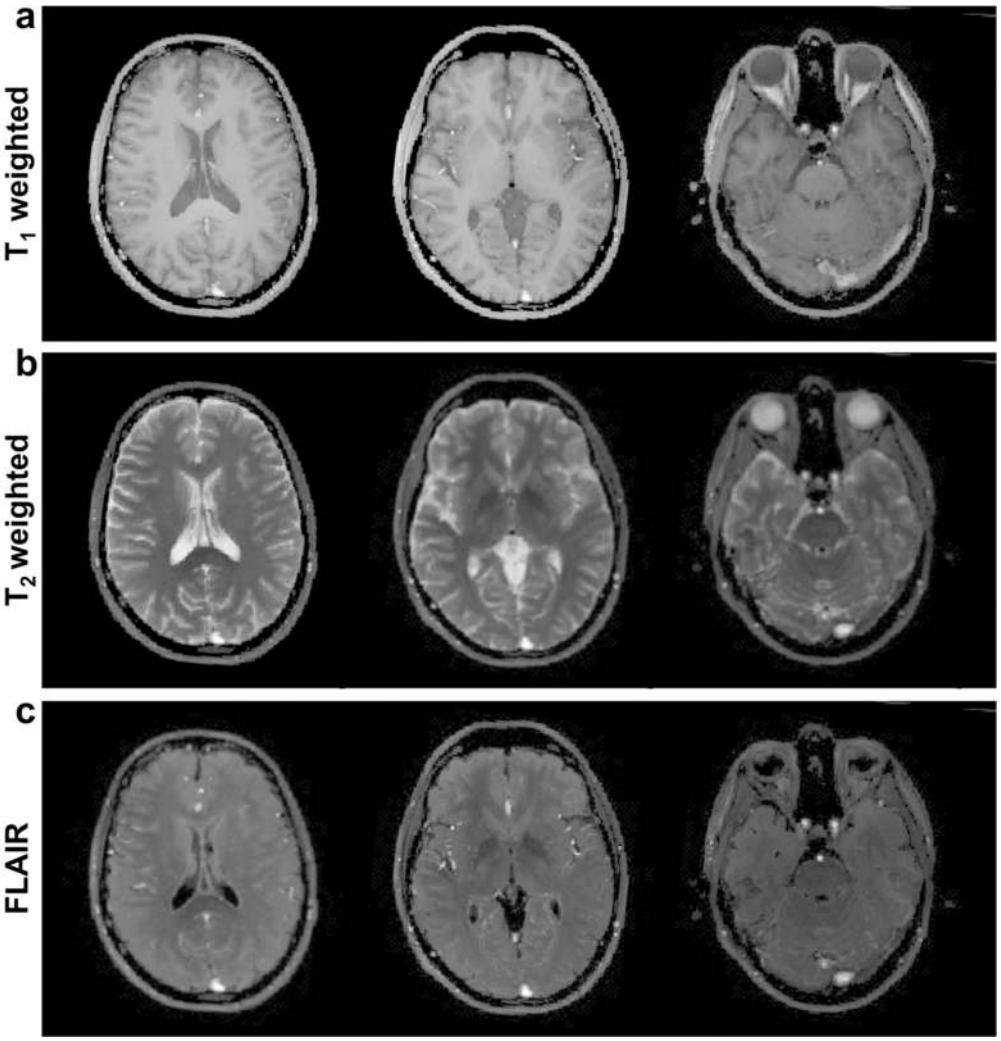

Figure 9.

a: T_1-weighted images calculated from the maps in Figure 8 with TR = 250 ms and TE = 2.5 ms; **b:** T_2-weighted images using TR = 10000 ms and TE = 90 ms and **c:** FLAIR images calculated with TI = 3600 ms, TE = 90 ms.

Author Manuscript

Author Manuscript

Author Manuscript

Author Manuscript

Table 1

T_1 and T_2 relaxation times and their standard deviations of MRF-FISP at 3 T, and the corresponding values reported in the literature (28).

			T_2 (*ms*)	T_2 (*ms*)
Tissue	**MRF-FISP**	**Literature (28)**	**MRF-FISP**	**Literature (28)**
White matter	781±61	788~898	65±6	78~80
Gray matter	1193±65	1286~1393	109±11	99~117